minerals

MDPI

Article

Mineral Chemistry of Low-Temperature Phyllosilicates in Early Paleozoic Metaclastic Rocks, Eastern Tauride Belt, Türkiye

Ömer Bozkaya [1,*] and Hüseyin Yalçın [2]

[1] Department of Geological Engineering, Pamukkale University, 20160 Denizli, Turkey
[2] Department of Geological Engineering, Sivas Cumhuriyet University, 58140 Sivas, Turkey
* Correspondence: obozkaya@pau.edu.tr

Abstract: The mineral chemistry of illite/mica and chlorites, together with the evaluation of textural data of low-temperature metaclastic rocks, plays an important role in determining their origin and metamorphic grade. This study aimed to investigate the chemical properties of phyllosilicates in early Paleozoic metaclastic rocks in the Eastern Tauride Belt, Türkiye. The textural (electron microscopy) and chemical (mineral chemistry analysis) analyses were performed on the samples representing different grades of metamorphism. The illites/micas and chlorites are observed as detrital (chlorite–mica stacks) and neoformation origin. Trioctahedral chlorites (chamosite) exhibit different chemistry for detrital and neoformed origin as well as the metamorphic grade. Tetrahedral Al and octahedral Fe + Mg increase, whereas octahedral Al decreases together with the increasing grade of metamorphism. The detrital chlorites have higher tetrahedral Al and Fe contents than their neoformed counterparts. Chlorite geothermometry data (detrital: 241–≥350 °C; neoformed: 201–268 °C) are compatible with the texture and illite Kübler index data. Illite/white-mica compositions display muscovite and Na-K mica. Tetrahedral Al and interlayer K + Na contents of illites/micas increase with metamorphic grade. Na-K mica and paragonite are observed as replacement-type developments within the detrital CMS. The obtained data indicate that phyllosilicate chemistry can be used effectively for determining the geological evolution of low-grade metamorphic sequences.

Keywords: phyllosilicate; mineral chemistry; metaclastic rocks; low-grade metamorphism

Citation: Bozkaya, Ö.; Yalçın, H. Mineral Chemistry of Low-Temperature Phyllosilicates in Early Paleozoic Metaclastic Rocks, Eastern Tauride Belt, Türkiye. *Minerals* **2022**, *12*, 1088. https://doi.org/10.3390/min12091088

Academic Editors: Iuliu Bobos and Franck Bourdelle

Received: 15 July 2022
Accepted: 25 August 2022
Published: 28 August 2022

1. Introduction

Phyllosilicates in diagenetic to very low-grade metamorphic sedimentary units exhibit textural and mineralogical features based on their occurrence in different tectonic and burial settings; they have the potential, therefore, to be used as indicators of time and temperature history [1,2]. The cleavage development is a common indicator for increasing temperature and pressure for extensional and compressional settings, whereas the observation of chlorite–mica stacks (CMS: [3,4]) or intergrown phyllosilicate grains [5], related to chloritization of detrital biotites, is a characteristic indicator of extensional basin activity (very-low grade metamorphism) [2].

Mineralogic (mineral assemblages, illite Kübler index, polytypes of K-micas and chlorite and *b* cell dimension of illite/white K-micas) studies of diagenetic to very low-grade metamorphic argillaceous sedimentary rocks have been used to reconstruct the thermal histories and the structural evolution of sedimentary basins and orogenic belts (i.e., [2,6–9]). In addition to mineralogical data, the chemistry of detrital and neoformed (authigenic) illite/mica and chlorites, forming the main components of metaclastic rocks, plays an important role in determining their origins and diagenetic–metamorphic grades, respectively. During the progressive transformation of illite to white K-mica, the interlayer K and tetrahedral charge increase due to Al^{3+} substitution for Si^{4+}, and the octahedral charge increases due to Fe^{2+} and Mg^{2+} substitution for Al^{3+} [10–12]. Chlorite composition is also sensitive to the diagenetic/metamorphic grade. The tetrahedral Al (Al^{IV}) and octahedral R^{2+} (Mg and

Fe^{2+}) contents of chlorite increase with increasing grade [13–20]. Thus, different chemical compositions for detrital (metamorphic) and authigenic (diagenetic) chlorites have been reported in many studies (e.g., [17,21–25]). During the last 10 years, semi-empirical methods using ratios of end-member activities to link chlorite composition to temperature through the equilibrium constant K [26–30] have been preferred for temperature estimations from diagenetic to very low-grade metamorphic chlorite compositions. Additionally, the new *T*–$R2^+$–Si diagram was also provided as a practical tool for thermometric, in particular for diagenesis and low-grade metamorphism [31], based on the chlorite solid-solution model.

The Tauride–Anatolide Platform or the Tauride–Anatolide Composite Terrain (TACT [32]), represents an Alpine continental microplate (Figure 1a). Surrounded by the northern and southern branches of the Neotethys, the TACT experienced crustal thickening related to the Latest Cretaceous Alpine closure of the Neotethyan ocean branches and subsequent collision with the surrounding continental microplates (e.g., [33]). The commonly accepted scenario for the evolution of the TACT is that nappes or tectonostratigraphic units at the northern margin of the platform were sliced and emplaced towards the south onto a relatively autochthonous central part (Geyik Dağı Unit, [34]). In contrast to the allochthonous units of the Taurides, the relatively autochthonous Geyik Dağı Unit contains better-preserved successions and a wide range of grades (diagenesis to epizone), in which Precambrian and Lower Paleozoic sedimentary sequences [35–37].

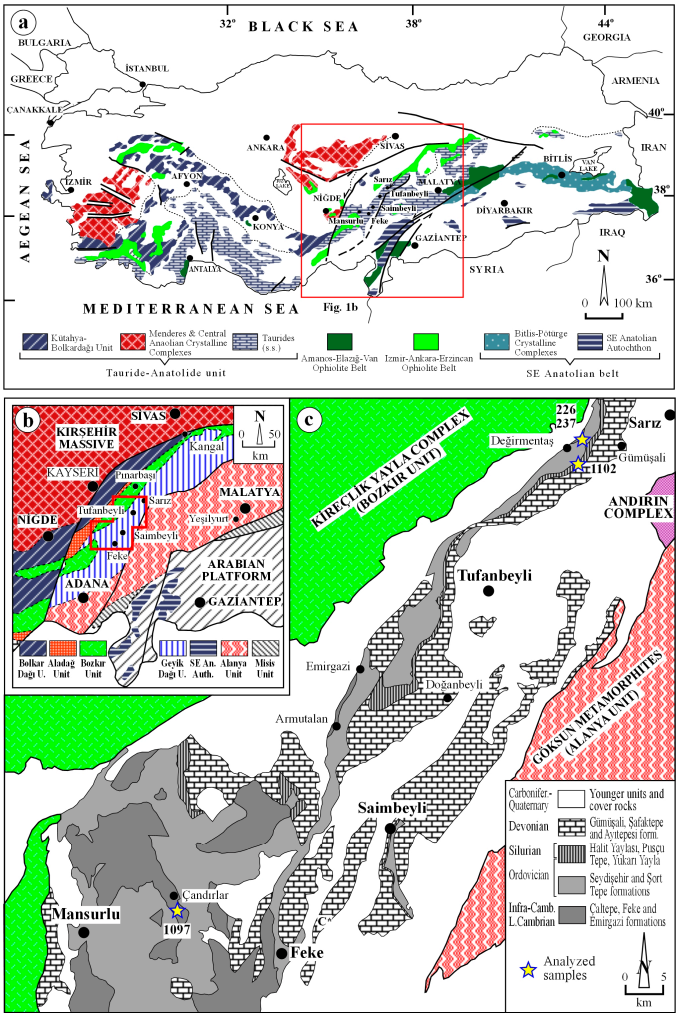

Figure 1. (**a**) Tectonic map of southern Turkey (Modified from [32]). (**b**) Tectono-stratigraphic units of the Eastern Tauride belt [34]. (**c**) Geologic map of the Geyik Dağı Unit between Sarız and Feke (simplified from [38]) and sample locations.

This study aimed to investigate the mineral chemistry of illites/micas and chlorites from the anchizonal to epizonal grade of the Precambrian–Early Paleozoic metaclastic sequence of the Geyik Dağı Unit. In this context, the obtained temperature conditions of neoformed and detrital phyllosilicate minerals correlate with the relationship between phyllosilicate chemistry and crystal–chemical data of phyllosilicates (illite Kübler index, polytype of illite/mica) which have been previously investigated by [36].

2. Geological Setting and Stratigraphy

Tectono-stratigraphic units of the TACT and their paleo-geographic setting relative to the autochthonous Geyik Dağı Unit are distinguished and differentiated by their stratigraphic and structural characteristics [34]. Based on the palinspastic reconstruction and interpretation of Özgül [34], the other units, called "allochthonous units", are palinspastically restored from north to south as the Bozkır Unit, Bolkar Dağı Unit, Aladağ Unit, and Alanya Unit in the Eastern Tauride Belt (Figure 1a,b).

The study area is located between Kayseri and Adana in the western part of the Eastern Taurides (Figure 1a,b). The Eastern Taurus Autochthonous Unit [38], or the eastern part of the Geyik Dağı Unit [34], shows a relatively well-exposed section in the Sarız–Tufanbeyli–Saimbeyli area (Figure 1c). In this area, the Geyik Dağı Unit is overthrusted by the Kireçlik Yayla Complex [39], Andırın Complex [38], and Göksun Metamorphites [40]. The Lower Paleozoic parts of the autochthonous units, which were investigated in this study, consist of Emirgazi, Feke, Çaltepe, Seydisehir, Sort Tepe, Halit Yaylası, Pusçu Tepe, Yukarı Yayla, and Ayı Tepesi formations from bottom to top.

The Emirgazi formation is composed of phyllitic slates and/or phyllites, alternating with metasiltstone, metasandstone, and rarely, recrystallized limestone (metalimestone). The Feke formation is mainly made up of purplish red colored metasandstones with yellow-green colored slate laminations. It overlies the Emirgazi formation as a parallel unconformity [41] and overlying by the Çaltepe formation, which is characterized, from bottom to top, by white-gray dolomite, dark gray recrystallized limestone, and green-pink nodular metalimestone of Upper Cambrian age. A transitional boundary exists to the overlying Seydişehir formation, which contains slate–metasiltstone alternations, intercalated with bands of recrystallized nodular limestone at the lower part and shales alternating with siltstones at the middle to the upper part.

The lower parts of the Seydişehir formation (Tremadocian parts) are brighter and more cleaved than the overlying Arenigian parts, and they show a distinct mineral orientation. After a stratigraphic gap including the middle Ordovician and probably the lower part of the Upper Ordovician, the shales of the Ashgillian Şort Tepe formation unconformably overly the Seydisehir formation. The late Ashgillian Halit Yaylası formation paraconformably overlies the Şort Tepe formation and is made up of glacial conglomerates [42] and sandstones, including silty shale alternations. The lower Silurian Pusçu Tepe formation contains shales and black shale–siltstone alternations. The Yukarı Yayla formation includes shales with limestone interlayers and was deposited during mid-Silurian. After a stratigraphic gap that may cover the Upper Silurian, the lower Devonian Ayı Tepesi formation unconformably covers the older units. It is followed by the middle Devonian Şafaktepe formation, represented by dolomitic limestone and limestone with sandstone–shale alternations. It is unconformably overlain by Gümüşali (upper Devonian) and Ziyarettepe (lower Carboniferous) formations, respectively.

3. Materials and Methods

Four rock samples from the Precambrian Emirgazi and Ordovician Seydişehir and Şort Tepe formations of the Eastern Tauride Belt Unit (Figure 1b,c) were selected for electron microscopy and mineral–chemistry analysis. Mineralogical–petrographic investigations using X-ray diffraction (XRD, Rigaku DMAX IIIC, Applied Rigaku Technologies, Austin, TX, USA) and optical microscopy (OM, Nikon, Tokyo, Japan), were previously carried out by [36] at the Geological Engineering Laboratory, Cumhuriyet University, Sivas, Turkey.

In this study, in addition to additional optical microscopic study, the electron microscopic mineral image (scanning electron microscope—secondary electrons and backscattered electrons/SEM-SE and SEM-BSE) and chemistry (energy dispersion spectrometry—EDS and electron microprobe-EMP) studies were performed on the polished and carbon coated surfaces on the samples.

SEM-SE and SEM-BSE images and EDS analyses were conducted at the Georgia Electron Microscopy (GEM) laboratory at the University of Georgia, Athens, GA, USA. The SEM investigations were performed using a Zeiss 1450EP instrument equipped with an Oxford INCA EDS system. This has a variable pressure sample chamber which allows imaging from high vacuum mode to 2600 Pa. The samples were coated with carbon and prepared as both freshly crushed grains (for SEM-SE images) and polished rock slabs (for SEM-BSE images). Thin-section slides were prepared using standard mounting techniques and polished to a thickness of 30 μm.

EMP analysis of minerals on carbon-coated polished rock slabs was performed with a JEOL 8600 electron microprobe using a 15 kV accelerating voltage and 15 nA beam current. Mineral grains were identified qualitatively using a Bruker 5010 Silicon Drift Detector (SDD) controlled by a Bruker Quantax energy dispersive analysis system. Quantitative analyses were performed with wavelength dispersive spectrometers (WDS) automated with Advanced Microbeam, Inc. EMP software, using 10 s counting times and natural and synthetic mineral standards. Analyses were calculated using Armstrong's Phi-Rho-Z matrix correction model [43,44]. The BSE and SE images and X-ray maps were acquired using the imaging software of the Quantax analysis system.

A total of 286 mineral chemistry analyses were conducted on micas/illites (117 EDS, 39 EMP) and chlorites (81 EDS, 49 EMP). Both EDS and EMP analyses of illite/mica and chlorites were performed on the same samples so that semi-quantitative EDS data could be calibrated with EMP data [25]. Thus, the EDS element oxide values were converted to EMP values, and these values could be used as EMP data.

4. Results

4.1. Texture

The main mineralogical–petrographical and textural characteristics of the Precambrian–Ordovician metaclastic rocks are given in Table 1. The grade of phyllosilicate orientation and cleavage developments in the matrix increases toward older units, i.e., from late Ordovician Şort Tepe formation to Precambrian Emirgazi formation (Figure 2).

Table 1. Optical mineralogical properties of the studied samples (Qz = Quartz, Pl = Plagioclase, Chl = Chlorite, Ms = Muscovite, Bt = Biotite, Tur = Tourmaline, Zrn = Zircon, Om = Opaque mineral.

Sample/ Formation	Rock Type/ Texture	Optical Mineralogy	Some Textural Properties
TFK-1097 Precambrian	Metasiltstone Blastopelitic	Qz + Pl + Ms + Chl + Om	Distinct orientation, roughly developed crenulation cleavage, scarce CMS are rich in muscovite
TTB-226 E.Ordovician	Chlorite slate Blastopelitic	Qz + Pl + Chl + Ms + Bt + Tur + Zrn + Om	Microlamination, distinct orientation, well-developed slaty cleavage, abundant CMS are rich in chlorite
TTB-237 E.Ordovician	Metasandstone Blastopsammitic	Qz + Pl + Chl + Ms + Tur + Zrn + Om	Abundant CMS are very rich in chlorite, distinct orientation, poorly-developed slaty cleavage
TTB-1102 L.Ordovician	Silty slate Blastopelitic	Qz + Fel + Ms + Om	Abundant CMS are rich in chlorite, less developed orientation formed from detrital CMS, mica and chlorite

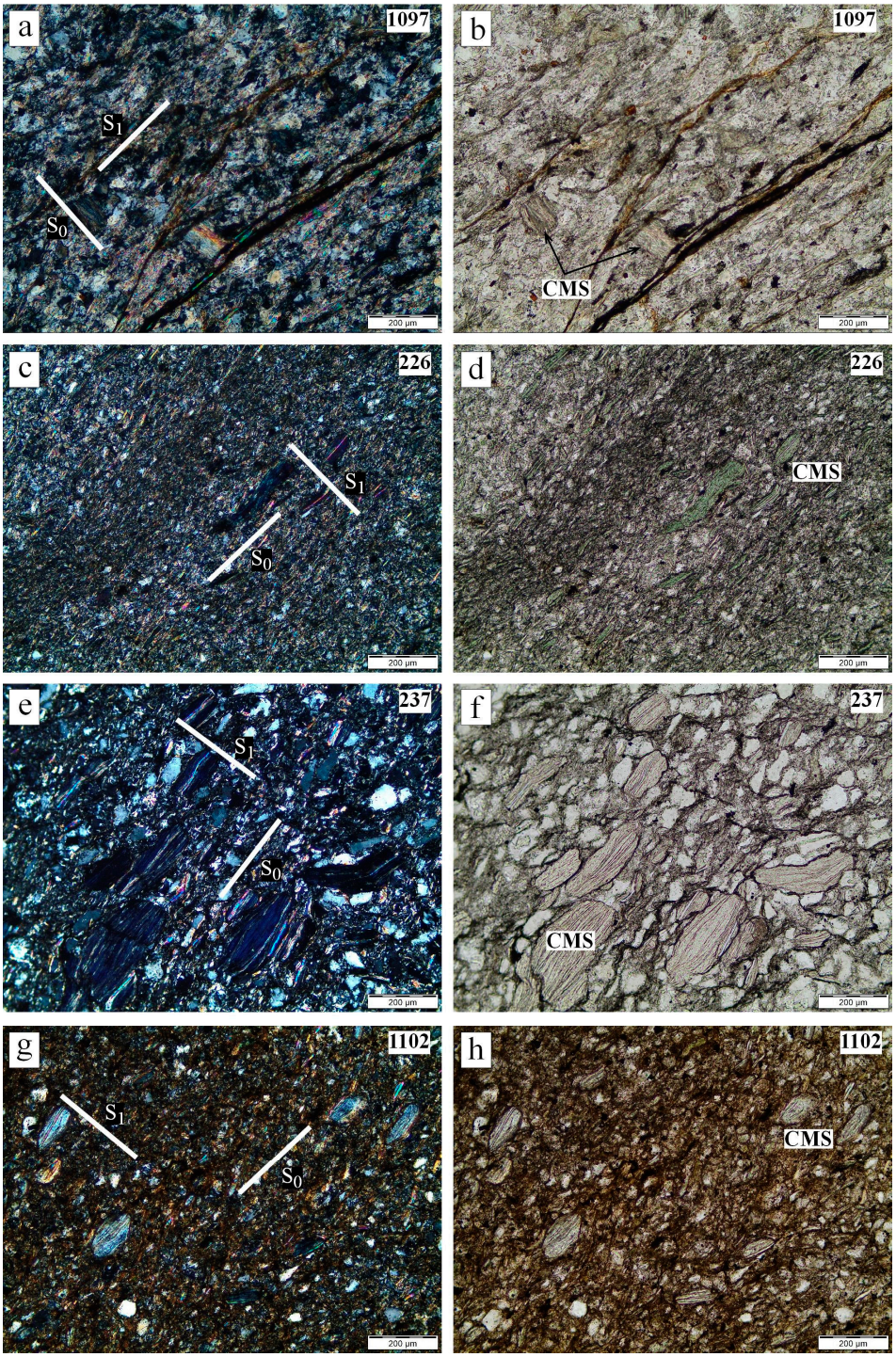

Figure 2. Photomicrographs of the Early Paleozoic siliciclastic rocks from the Geyik Dağı Unit in the Eastern Tauride Belt. Photos on the left were taken under crossed nicols, and on the right were taken under plane-polarized light. (**a**,**b**) Detrital CMS parallel to bedding planes (S_0) and perpendicular to slaty cleavage planes (S_1) in metasiltstone from Precambrian Emirgazi formation. (**c**,**d**) Chlorite-rich CMS; their long axes are parallel to S_0 and perpendicular to S_1 in chlorite slate from lower parts of early Ordovician Seydişehir formation, (**e**,**f**) Abundant chlorite-rich CMS which is parallel to S_0 in the anchimetamorphic sandstone from the lower–middle part of the Seydişehir formation, (**g**,**h**) White K-mica-rich CMS in silty slate from the late Ordovician Şort Tepe formation.

Optical microscopic investigations of the Precambrian and Ordovician siliciclastic rocks revealed distinctive bedding orientations (S_0), formed by chloritized and illitized groundmass and coarse detrital mica flakes, and poorly developed cleavage planes (S_1) which are nearly perpendicular to S_0 (Figure 2a–h). The schistosity and cleavage development in the samples increased from the late Ordovician to the Precambrian, together with an increasing degree of diagenesis/metamorphism. Intense chloritization of biotite and lozenge-shaped CMS are encountered in all samples.

Detrital mineral (quartz and plagioclase) boundaries are sutured with a groundmass of fine-grained micas (sericite) and chlorites in the Precambrian phyllitic slate sample (Figure 2a,b). Chloritization of coarse-grained biotite and the presence of chlorite-bearing mica stacks suggest that detrital biotite was altered under very low-grade metamorphic conditions [45,46]. Similar features for early Paleozoic units were also noted in the western and central Taurides [25,47]. CMS in the Precambrian lower parts of the Seydişehir formation are rich in chlorite components (Figure 2c–g), whereas CMS in the Emirgazi and Şort Tepe formation have relatively low chlorite content (Figure 2a,b,g,h) and some stacks in the Emirgazi formation consist almost entirely of white micas (Figure 2a,b).

The SEM-SE images of the phyllitic slate sample show that chlorite–muscovite–NaK mica stacks are highly deformed and their long axes were almost angularly oriented to the cleavage and/or shear zones (Figure 3a,b). The groundmass consists of relatively fine-grained flaky white K-mica and neoformed chlorites. Neoformed illite and chlorites were developed in voids and pores as fine-grained aggregates (Figure 3c). Neoformed illites were also developed onto coarse-grained muscovite plates (Figure 3d).

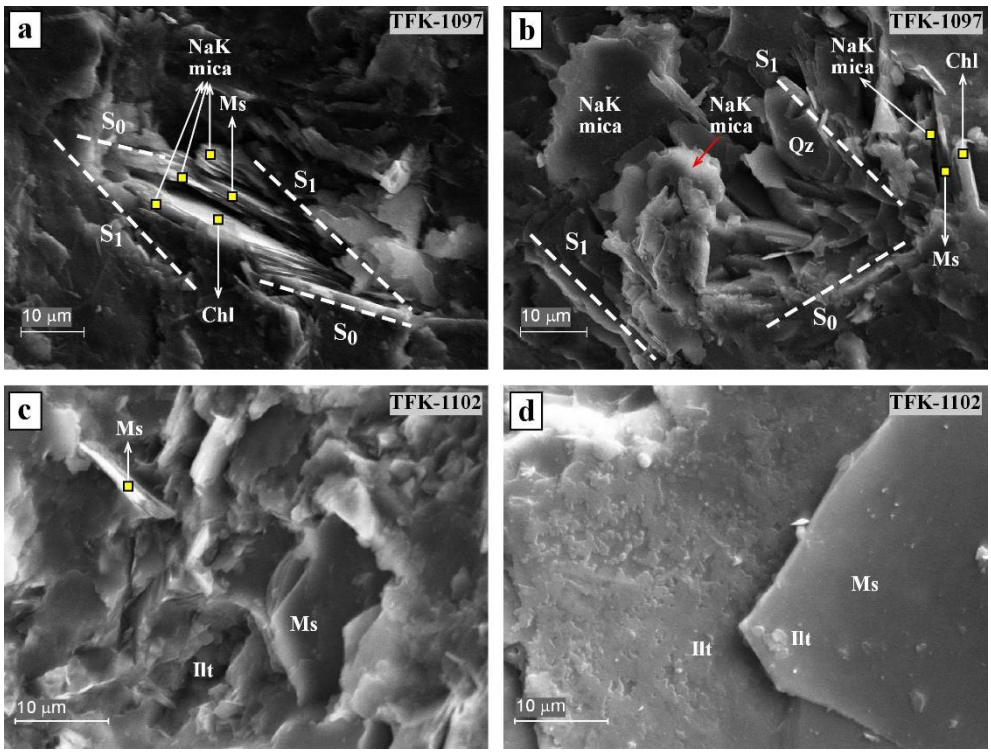

Figure 3. SEM-SE photomicrographs of the Precambrian and late Ordovician metapelitic rocks from the Eastern Tauride Autochthon. (**a**,**b**) Chlorite–muscovite–NaK mica stack showing its stacking planes are parallel to bedding plane (S_0) and high angle to cleavage (shear) planes (S_1). (**c**,**d**) The association of detrital micas and neoformed illites, which developed in voids and pores and onto the coarse-grained muscovite plates, as well.

The SEM-BSE images of the metasiltstone sample of Precambrian Emirgazi formation exhibit coarse-grained CMS. The stacking planes of chlorite-rich CMS were distinctly

oriented as parallel to bedding planes (Figure 4a,b), whereas stacking planes of white mica-rich CMS, developed alongside the tectonically disturbed zones (syn-tectonic origin), were nearly perpendicular to bedding planes which were also parallel to shear planes (Figure 4c–f). White mica-rich and strongly disturbed CMS also contained the replacement-type NaK-micas within the stacks (Figure 4e,f), as demonstrated by the X-ray elementary map data (Figure 4g–j). Pore-filling neoformed illites and chlorites developed with a non-oriented texture, suggesting post-tectonic formation during a later (post-tectonic) phase. Additionally, the neoformed phyllosilicates were also developed on the coarse mica and chlorites less frequently.

The SEM-BSE photomicrographs of the slate sample of the early Ordovician part of the Seydişehir formation show that the long axes of CMS have a distinctly oriented parallel to the bedding planes (Figure 5a–f). CMS are generally chlorite-rich and coarse-grained (the lengths of the stacks reach 300 μm and their thickness reaches 100 μm) and tectonically disturbed in places (Figure 5a,c). The neoformed illites and chlorites were developed in the pores of the groundmass having partial orientation.

The SEM-BSE images of the metasandstone sample of the late–early Ordovician part of the Seydişehir formation exhibit coarse (>100 μm) CMS composed of almost chlorite components, including thin white K-mica layers in rare amounts (Figure 6a–f). Elongated and lozenge-shaped CMS have stacking planes nearly parallel to bedding planes and are partly disturbed due to cutting by slightly developed cleavage planes in places (Figure 6b,f).

The SEM-BSE photomicrographs of the late Ordovician silty slate display distinct orientation formed by CMS and detrital micas and chlorites (Figure 7a–f). Elongated and lozenge-shaped CMS are rich in chlorite components and relatively less deformed with respect to the other samples (Figure 7a–c,f). The groundmass is formed from fine-grained quartz grains and pore-filling neoformed phyllosilicates (illites and chlorites) without orientation.

4.2. Mineralogy

Bulk and phyllosilicate fraction and crystal–chemical data (illite Kübler index, $\Delta^{\circ}2\theta$, [48]) polytype, and *b* cell dimension of illite/muscovite), which were previously studied by the current authors [36], are given in Figure 8. The main mineralogical composition is, in the order of abundance, phyllosilicates, quartz, alkali feldspar, plagioclase, and small amounts of calcite and dolomite. The amounts of quartz are increased in the Halit Yaylası formation, of feldspar in the Emirgazi and Feke formations, and of carbonates in the Çaltepe and Yukarı Yayla formations, depending on the main lithological types (metacarbonates and carbonate rocks are composed of calcite, dolomite, and detrital clasts such as quartz, plagioclase, and phyllosilicates). With respect to their relative amounts, phyllosilicates show a wide variety in mineral contents of illite, chlorite, mixed-layered chlorite–vermiculite (C-V), chlorite–smectite (C-S), illite–smectite (I-S), PM, and paragonite.

In terms of the vertical distribution of the phyllosilicates, illite/muscovite is found in all units. Chlorite is mostly detected in the Cambrian–Ordovician, while C-V occurs in the Silurian–Devonian and the Cambrian earliest Ordovician. C-S, PM, and paragonite are only detected in the Emirgazi formation, while I-S is only observed in the Ayı Tepesi formation (Figure 8). Increasing amounts of chlorite and illite but decreasing C-V and I-S towards depth is related to progressive evolution with stratigraphic depth, as stated by [36].

According to illite Kübler index data, Precambrian to early Ordovician units have epimetamorphic, early–middle Ordovician to middle Silurian, and late Silurian to early Devonian have anchimetamorphic and high-grade diagenetic degrees (Figure 8). The $d_{(060)}$ or b_0 values of illites and $2M_1$-contents ($2M_1/[2M_1 + 1M_d]$) of illite increase from Devonian to Ordovician formations.

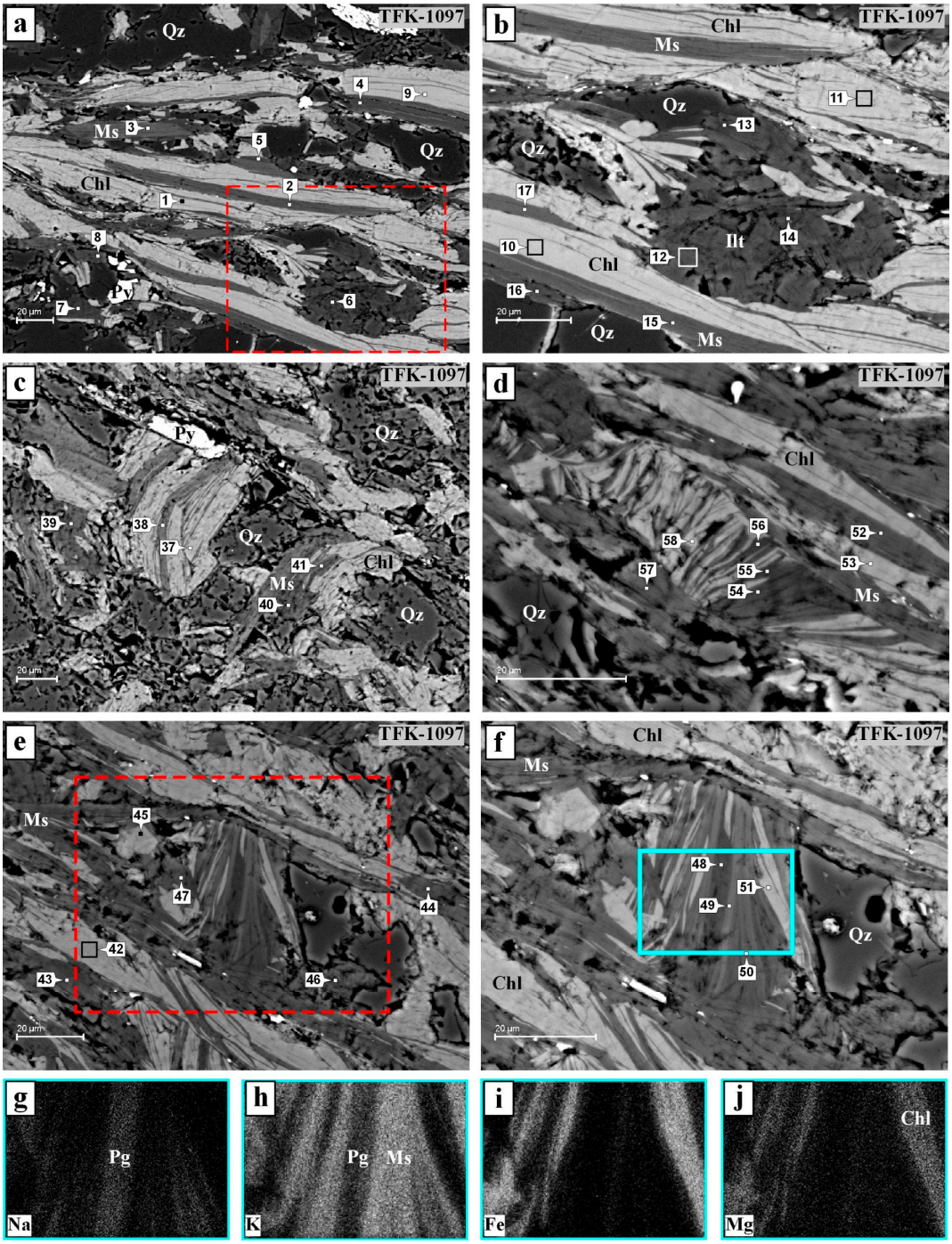

Figure 4. SEM-BSE photomicrographs of the Precambrian phyllitic slate with locations of some analyzed points and areas (black rectangulars). (**a**,**b**) Coarse-grained CMS oriented their long axes along the bedding planes and post-metamorphic illite occurrences, (**c**,**d**) The associations of CMS; both their stacking {001} planes are parallel to bedding planes and {001} are nearly perpendicular to bedding planes, i.e., along the schistosity or cleavage planes, (**e**,**f**) Highly disturbed white mica-rich CMS between shear zones in which {001} planes of CMS are nearly perpendicular to bedding plane and also to the shear band planes, (**g**–**j**) X-ray elementary maps (Na, K, Fe, Mg) of the CMS displaying the chemical differences of chlorite, white K- and Na-K mica/paragonite. Chl = Chlorite, Ilt = Illite, Ms = Muscovite, Pg = Paragonite, Py = Pyrite, Qz = Quartz.

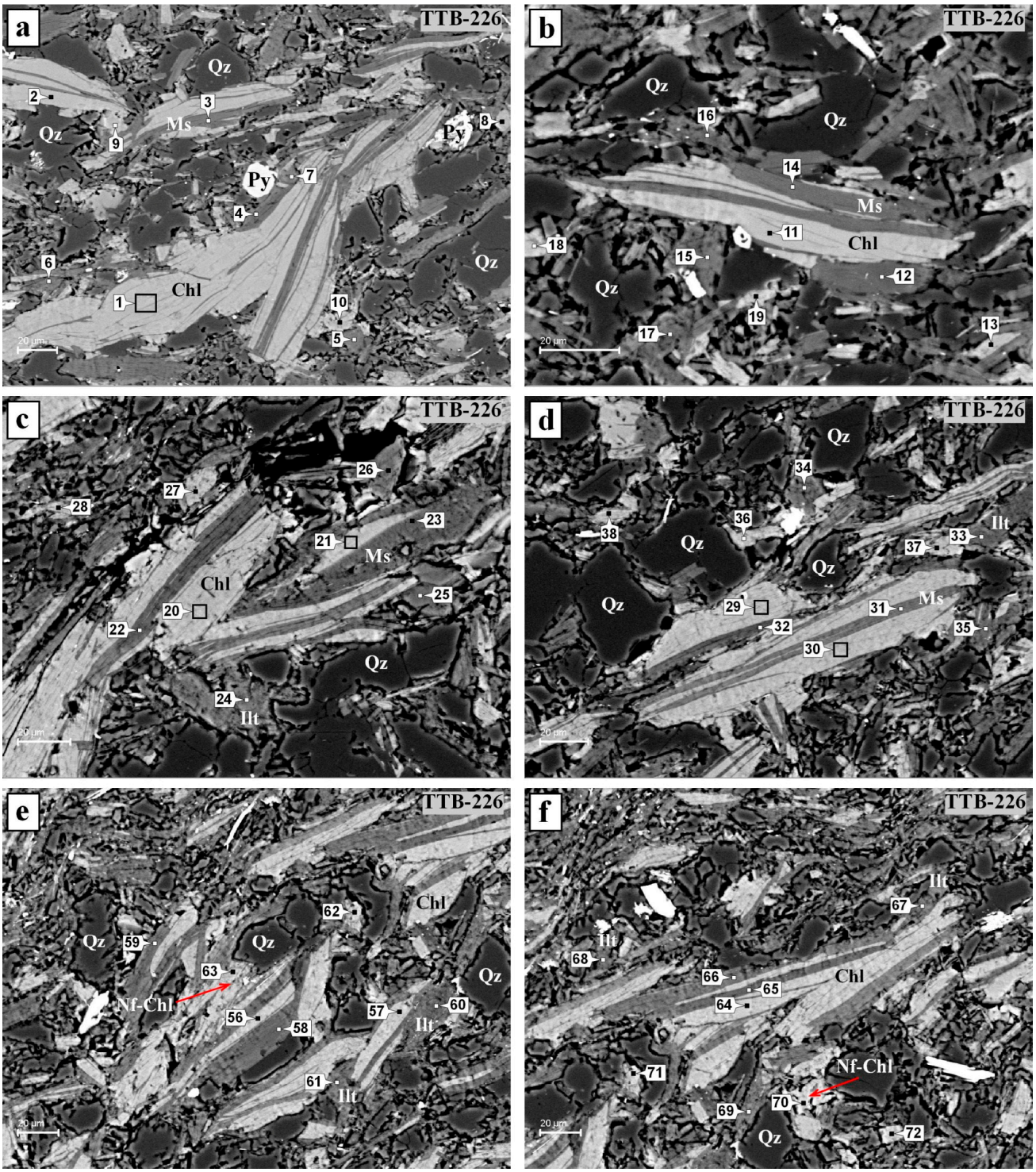

Figure 5. SEM-BSE photomicrographs of the early Ordovician slate with locations of some analyzed points and areas (black rectangulars). (**a**,**b**) Coarse-grained tectonically disturbed chlorite-rich CMS which parallel the bedding planes within the slightly oriented groundmass, (**c**,**d**) Chlorite-rich CMS within the quartz, neoformed illite (Ilt) and chlorite (Nf-Chl) bearing groundmass, (**e**,**f**) Muscovite-rich CMS with long axes were almost parallel to bedding planes and widespread occurrences of neoformed illites and chlorites in the pores of the groundmass. Chl = Chlorite, Nf-Chl: Neoformed chlorite, Ilt = Illite, Ms = Muscovite, Py = Pyrite, Qz = Quartz.

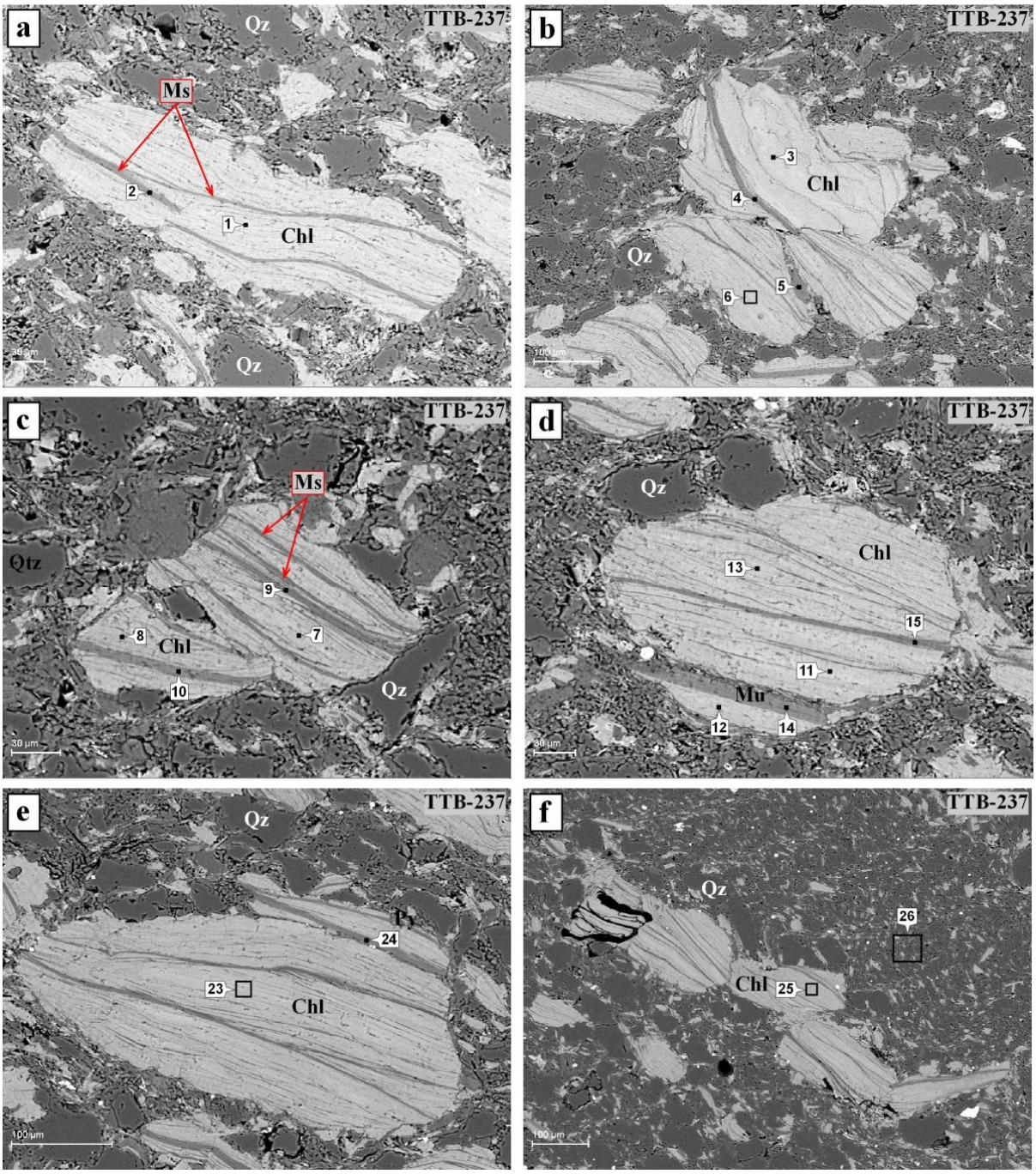

Figure 6. SEM-BSE photomicrographs of the early–middle Ordovician metasandstone with locations of some analyzed points and areas (black rectangulars). (**a**) Elongated chlorite-rich CMS which their stacking planes are nearly parallel to bedding planes and partly disturbed due to cutting by slightly developed cleavage planes, (**b**–**e**) Lozenge-shaped chlorite-rich CMS cutting by cleavage planes, (**f**) Elongated chlorite-rich CMS which multiple sliced by slightly developed cleavage planes within the groundmass composed of quartz-fine grained-white K-mica and chlorite.

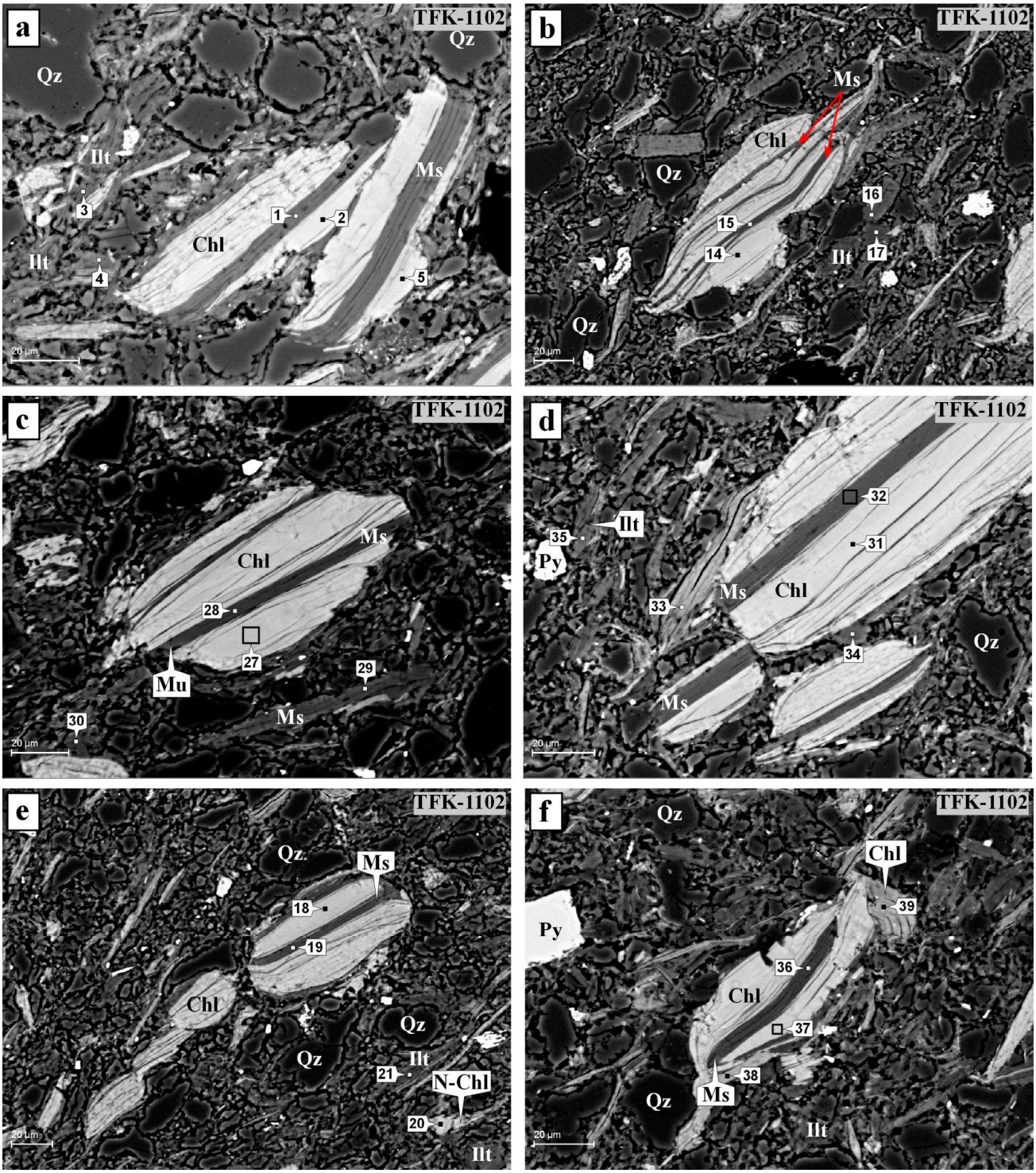

Figure 7. SEM-BSE photomicrographs of the late Ordovician silty slate with locations of some analyzed points and areas (black rectangulars). (**a**) Elongated chlorite-rich CMS which their stacking planes nearly parallel to bedding planes within the groundmass, including neoformed illites and chlorites, (**b**,**c**) Lozenge-shaped and curved chlorite-rich CMS, (**d**,**e**) Elongated chlorite-rich CMS, their long axes are parallel to bedding planes and sliced by crenulation type of cleavage planes in the quartz-fine grained-white K-mica and chlorite groundmass, (**f**) Elongated and curved chlorite-rich CMS within the groundmass containing pore filled neoformed illites and chlorites.

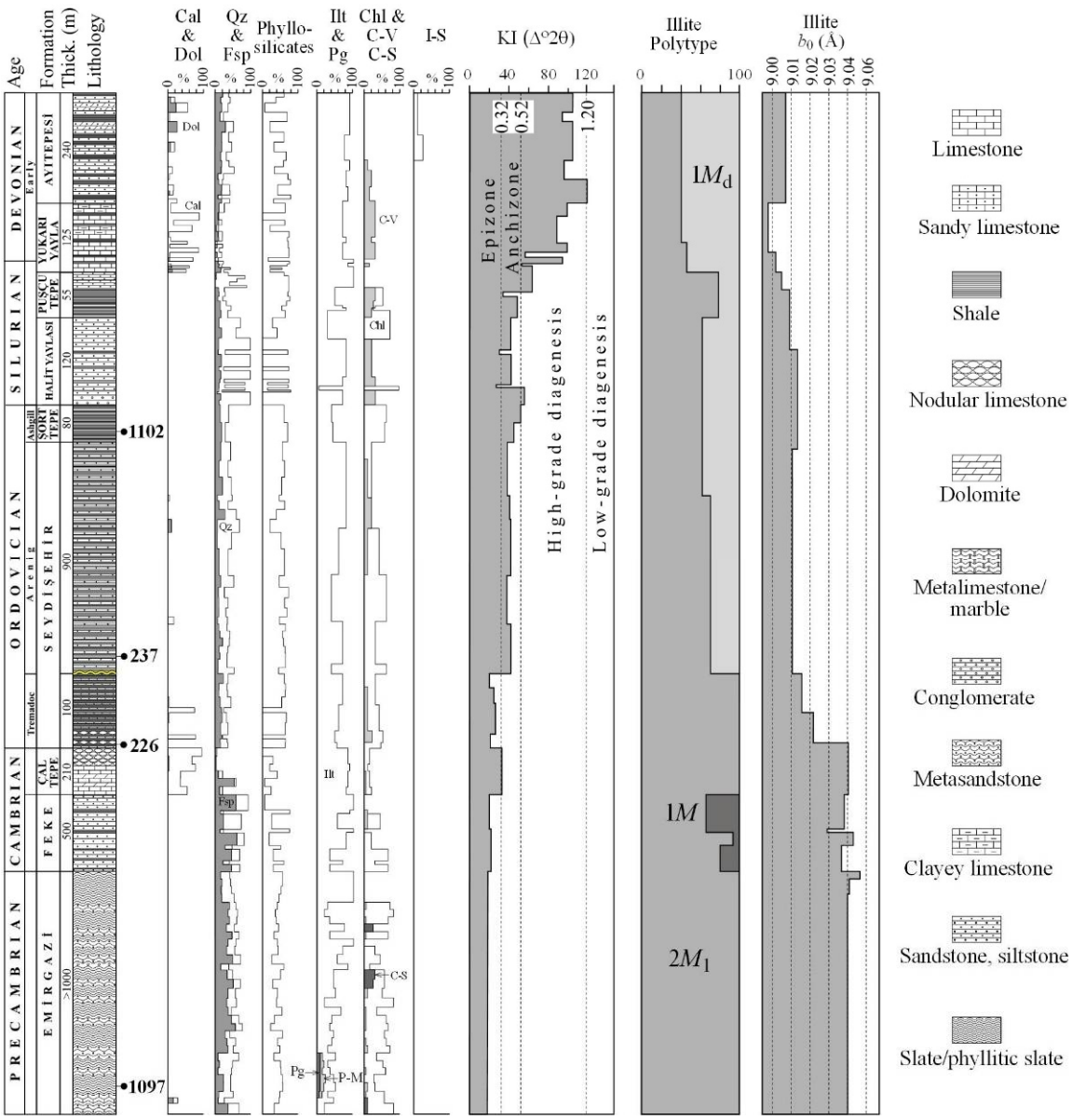

Figure 8. Vertical distribution of mineralogic data in the Lower Paleozoic units (Modified from [36]). Cal = Calcite, Chl = Chlorite, Dol = Dolomite, Fsp = Feldspar, Ilt = Illite, I-S = Mixed-layered illite-smectite, Ms = Muscovite, Pg = Paragonite, Qz = Quartz, C-S = Mixed-layered chlorite–smectite, C-V = Mixed-layered chlorite–vermiculite, KI = Illite Kübler index.

There is a positive correlation among % KI, $2M_1$%, and b_0 of illites/micas, indicating that the diagenetic–metamorphic characteristics were mainly caused by sedimentary burial at the initial site of deposition in the Lower Paleozoic part of the Eastern Taurus Autochthonous Unit [36]. The increasing $2M_1$-contents and b_0 values of the illites refer to increasing temperature and pressure conditions toward the lower part, respectively [2,6–8].

The XRD data of studied samples are made up mainly of quartz, feldspar (plagioclase), and phyllosilicates (Figure 9, Table 2 [36]). Phyllosilicate minerals of the samples are mainly represented by illite/muscovite, chlorite, and scarce mixed-layer chlorite–vermiculite (C-V).

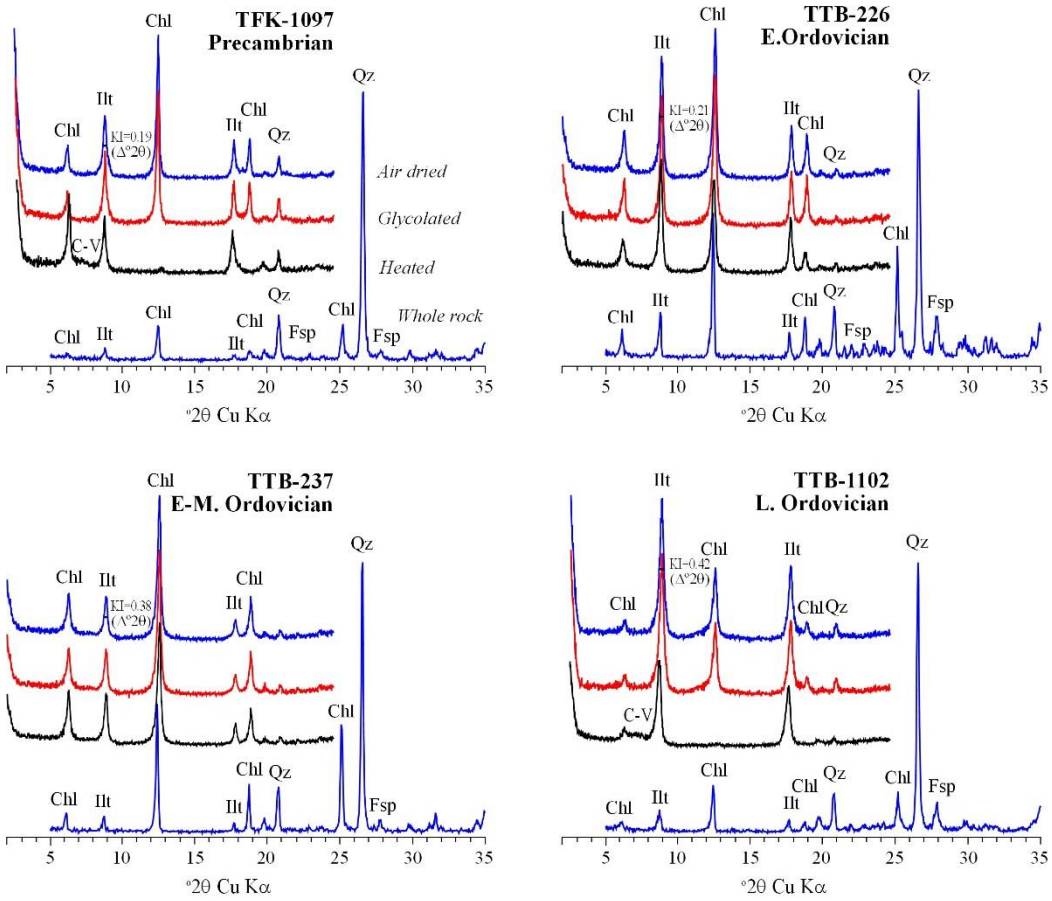

Figure 9. XRD patterns of whole rock and clay fraction of Precambrian–Ordovician metaclastic rocks. Chl = Chlorite, Fsp = Feldspar, Ilt = Illite, Ms = Muscovite, Qz = Quartz, C-V = Mixed-layer chlorite–vermiculite, KI = Illite Kübler index.

Table 2. Bulk and clay/phyllosilicate mineral composition and crystal–chemical data of illites of studied samples.

Sample/ Formation	Whole Rock			Clay Fraction				Crystal–Chemical Data			
	Qz	Fsp	Phl	Ilt	Chl	C-V	Pg-PM	KI	b_0	$2M_1$	$1M_d$
TFK-1097 Precambrian	40	8	52	35	50	5	10	0.19		100	
TTB-226 E.Ordovician	20	15	65	55	45			0.21	9.041	100	
TTB-237 E.Ordovician	27	6	67	30	70			0.38	9.023		
TTB-1102 L.Ordovician	29	22	49	55	35	10		0.42		90	10

Qz = Quartz, Fsp = Feldspar, Phl = Phyllosilicate, Ilt = Illite, Chl = Chlorite, C-V = Mixed-layered chlorite–vermiculite, Pg = Paragonite, PM = NaK mica, KI = Illite Kübler index, $2M_1$ = 2 layers monoclinic polytype, $1M_d$ = Disordered 1 layer monoclinic polytype.

KI (Δ°2θ) data of the samples correspond to epizone (TFK-1097, TTB-226), high- (TTB-237) and low-anchizone (TTB-1102) grades (Table 2). *b*0 (Å) values of illites/micas indicate the moderate to high pressure facies series [49,50]. The dominance of $2M_1$ polytype illite/mica contents corresponds to anchizonal-epizonal grades [6,7]. The phyllosilicate associations and crystal–chemical data exhibit reasonable compatibility for increasing

diagenetic/metamorphic grades, together with increasing sedimentary burial, from late Ordovician to Precambrian.

4.3. Mineral Chemistry

Average major element compositions obtained from EMPA and EDS data and structural formulae of phyllosilicates are listed in Tables 3 and 4 for chlorites and illites/micas, respectively. Unit-cell compositions were calculated on the basis of 11 oxygen equivalents for I-S and illite–mica and 14 oxygen equivalents for chlorite [51].

Table 3. Average chemical composition and structural formulae of chlorites of the early Paleozoic rocks from the Eastern Tauride Belt (CMS: Chlorite–mica stacks, NFC: Neoformed chlorites).

	EMP				EDS						
Sample	**TFK-1097**	**TTB-226**	**TTB-237**	**TTB-1102**	**TFK-1097**	**TTB-226**	**TTB-226**	**TTB-237**	**TTB-237**	**TTB-1102**	**TTB-1102**
Origin	**CMS**	**CMS**	**CMS**	**CMS**	**CMS**	**CMS**	**NFC**	**CMS**	**NFC**	**CMS**	**NFC**
(*n*)	**(5)**	**(12)**	**(6)**	**(5)**	**(16)**	**(15)**	**(18)**	**(13)**	**(2)**	**(11)**	**(3)**
SiO_2	22.47	24.46	23.89	22.38	26.27	28.52	29.40	26.90	29.24	26.01	30.08
TiO_2	0.02	0.04	0.29	0.02	0.00	0.00	0.00	0.00	0.00	0.00	0.00
Al_2O_3	24.97	21.75	24.96	24.28	28.34	25.73	25.22	28.90	27.58	27.65	25.35
FeO_{tot}	26.26	27.03	26.44	31.50	33.80	31.36	30.48	32.19	31.37	38.11	31.67
MnO	0.17	0.15	0.14	0.09	0.00	0.00	0.00	0.00	0.00	0.00	0.00
MgO	11.65	12.07	9.74	7.21	11.60	14.39	14.89	12.01	11.80	8.22	12.71
CaO	0.01	0.01	0.00	0.01	0.00	0.00	0.00	0.00	0.00	0.00	0.00
Na_2O	0.01	0.01	0.02	0.02	0.00	0.00	0.00	0.00	0.00	0.00	0.00
K_2O	0.00	0.00	0.01	0.00	0.00	0.00	0.00	0.00	0.00	0.00	0.18
Total	85.56	85.51	85.49	85.50	100.00	100.00	100.00	100.00	100.00	100	100
Si	2.45	2.67	2.59	2.51	2.48	2.66	2.72	2.52	2.71	2.51	2.80
Al^{IV}	1.55	1.33	1.41	1.49	1.52	1.34	1.28	1.48	1.29	1.49	1.20
Al^{VI}	1.65	1.47	1.78	1.72	1.64	1.49	1.48	1.70	1.72	1.66	1.58
Ti	0.00	0.00	0.02	0.00	0.00	0.00	0.00	0.00	0.00	0.00	0.00
Fe^{2+}	2.39	2.47	2.40	2.95	2.67	2.44	2.36	2.52	2.43	3.08	2.46
Mn	0.01	0.01	0.01	0.01	0.00	0.00	0.00	0.00	0.00	0.00	0.00
Mg	1.89	1.96	1.57	1.20	1.63	2.00	2.06	1.67	1.63	1.18	1.76
OC	1.54	1.32	1.40	1.48	1.52	1.34	1.28	1.48	1.29	1.49	1.18
TOC	5.94	5.92	5.79	5.88	5.94	5.93	5.90	5.89	5.78	0.00	0.00
Ca	0.00	0.00	0.00	0.00	0.00	0.00	0.00	0.00	0.00	0.00	0.00
Na	0.00	0.00	0.00	0.00	0.00	0.00	0.00	0.00	0.00	0.00	0.00
K	0.00	0.00	0.00	0.00	0.00	0.00	0.00	0.00	0.00	0.00	0.02
ILC	0.00	0.00	0.01	0.01	0.00	0.00	0.00	0.00	0.00	0.00	0.00
TLC	0.00	0.00	0.01	0.01	0.00	0.00	0.00	0.00	0.00	0.00	0.00
°C	>350	343	241	318	>350	343	268	321	204	>350	201

OC = Octahedral Charge, TOC = Total Octahedral Cation, ILC = Interlayer Charge, TLC = Total Layer Charge, *n* = number of analyses.

The mineral chemistry data of chlorites in the early Paleozoic metaclastic rocks (Table 3) show moderately narrow distributions of Si–R^{2+} and Al^{IV}–Fe/(Fe + Mg) diagrams (Figure 10). However, the compositions of chlorites in CMS and neoformed ones range among clinochlore/daphnite, amesite and sudoite end-members, almost places between clinochlore/daphnite and amesite (Figure 10a,b). Both neoformed and detrital (CMS) chlorites of the sample in early Ordovician (Tremadocian) parts exhibit reasonably different compositions than others because of the higher Si and R^{2+} contents. Neoformed chlorites have higher Si contents than those of detrital (CMS) chlorites. Although the chlorites are shown to have brunsvigite-ripidolite composition in the Al^{IV}–Fe/(Fe + Mg) diagram (Figure 10c,d), in accordance with AIPEA nomenclature [52], the Fe/(Fe + Mg) content of chlorites indicate the chamosite composition (Fe/(Fe + Mg > 0.5). The detrital chlorites have higher Al^{IV} and Fe contents than their neoformed counterparts.

Table 4. Average chemical composition and structural formulae of illite/micas of the early Paleozoic rocks from the Eastern Tauride Belt (Ms = Muscovite, Ilt = Illite, P-M = Paragonite-muscovite).

	EMP						EDS										
Sample	**1097**	**1097**	**226**	**237**	**1102**	**1102**	**1097**	**1097**	**1097**	**226**	**226**	**226**	**237**	**237**	**1102**	**1102**	**1102**
Origin	**Ms**	**Ilt**	**Ms**	**Ms**	**Ms**	**Ilt**	**Ms**	**Ilt**	**P-M**	**Ms**	**Ilt**	**P-M**	**Ms**	**Ilt**	**Ms**	**Ilt**	**P-M**
(*n*)	**(3)**	**(1)**	**(6)**	**(4)**	**(3)**	**(1)**	**(14)**	**(16)**	**(11)**	**(10)**	**(22)**	**(5)**	**(9)**	**(3)**	**(11)**	**(10)**	**(2)**
SiO_2	45.44	46.60	45.46	44.99	45.04	44.90	47.87	48.65	47.97	49.13	50.08	48.10	47.58	50.07	49.65	49.38	48.17
TiO_2	0.30	0.22	0.55	1.37	0.54	0.42	0.00	0.00	0.00	0.00	0.00	0.00	0.00	0.00	0.00	0.00	0.00
Al_2O_3	37.67	37.14	33.32	34.84	35.45	35.31	38.28	41.03	40.56	35.67	34.39	38.28	37.51	35.59	35.37	37.79	37.58
FeO_{tot}	0.93	0.81	2.49	3.07	2.93	0.83	2.43	0.68	2.48	2.82	3.62	1.79	3.14	2.51	2.75	1.75	3.00
MnO	0.03	0.01	0.07	0.05	0.06	0.01	0.00	0.00	0.00	0.00	0.00	0.00	0.00	0.00	0.00	0.00	0.00
MgO	0.60	0.68	1.55	1.15	0.92	1.82	1.36	0.55	1.06	1.91	1.93	1.46	1.68	1.79	2.09	1.43	1.69
CaO	0.01	0.02	0.02	0.01	0.05	0.05	0.00	0.00	0.00	0.00	0.00	0.00	0.00	0.00	0.00	0.00	0.00
Na_2O	0.80	1.23	0.50	0.33	0.64	0.44	0.95	2.23	3.91	0.58	0.27	1.28	0.60	0.35	0.45	0.32	1.49
K_2O	7.77	7.35	9.47	8.67	7.65	9.65	9.11	6.86	4.02	9.89	9.70	9.09	9.49	9.69	9.68	9.32	8.07
Total	93.55	94.07	93.44	94.50	93.28	93.43	100.00	100.00	100.00	100.00	100.00	100.00	100.00	100.00	100.00	100.00	100.00
Si	3.02	3.07	3.09	3.02	3.04	3.03	3.02	3.01	2.97	3.12	3.18	3.03	3.02	3.16	3.14	3.10	3.04
Al^{IV}	0.98	0.93	0.91	0.98	0.96	0.97	0.98	0.99	1.03	0.88	0.82	0.97	0.98	0.84	0.86	0.90	0.96
Al^{VI}	1.98	1.96	1.77	1.78	1.86	1.84	1.87	2.00	1.93	1.78	1.75	1.87	1.83	1.80	1.78	1.89	1.83
Ti	0.02	0.01	0.03	0.07	0.03	0.02	0.00	0.00	0.00	0.00	0.00	0.00	0.00	0.00	0.00	0.00	0.00
Fe^{2+}	0.05	0.04	0.14	0.17	0.17	0.05	0.13	0.04	0.13	0.15	0.19	0.09	0.17	0.13	0.15	0.09	0.16
Mn	0.00	0.00	0.00	0.00	0.00	0.00	0.00	0.00	0.00	0.00	0.00	0.00	0.00	0.00	0.00	0.00	0.00
Mg	0.06	0.07	0.16	0.12	0.09	0.18	0.13	0.05	0.10	0.18	0.18	0.14	0.16	0.17	0.20	0.13	0.16
OC	0.21	0.15	0.02	0.19	0.21	0.07	0.13	0.18	0.24	0.01	0.00	0.08	0.14	0.02	0.02	0.12	0.13
TOC	2.10	2.08	2.10	2.14	2.15	2.09	2.13	2.09	2.16	2.11	2.13	2.10	2.15	2.11	2.12	2.11	2.15
Ca	0.00	0.00	0.00	0.00	0.00	0.00	0.00	0.00	0.00	0.00	0.00	0.00	0.00	0.00	0.00	0.00	0.00
Na	0.10	0.16	0.07	0.04	0.08	0.06	0.12	0.27	0.47	0.07	0.03	0.16	0.07	0.04	0.06	0.04	0.18
K	0.66	0.62	0.82	0.74	0.66	0.83	0.73	0.54	0.32	0.80	0.79	0.73	0.77	0.78	0.78	0.75	0.65
ILC	0.76	0.78	0.89	0.79	0.75	0.90	0.85	0.81	0.79	0.87	0.82	0.89	0.84	0.82	0.84	0.79	0.83
TLC	0.76	0.78	0.89	0.79	0.75	0.90	0.85	0.81	0.79	0.87	0.82	0.89	0.84	0.82	0.84	0.79	0.83

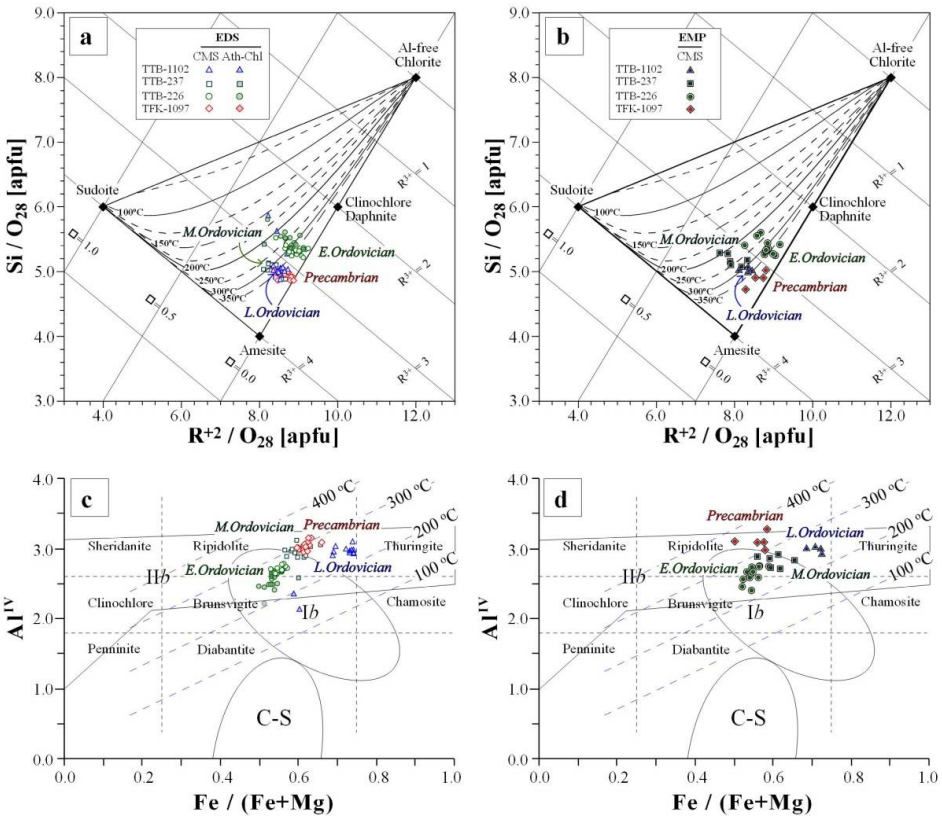

Figure 10. Distribution of chlorite compositions on (**a**,**b**) Si vs. R^{2+} (simplified from [53]), and (**c**,**d**) Al^{IV} vs. Fe/(Fe + Mg) diagram (modified from [54]; IIb chlorite area and compositional limits from [55]; Ib and swelling chlorites (C-S) areas from [56]. (**a**,**c**) and (**b**,**d**) represent the analytical results by EDS and EMP, respectively. Temperature contours on Si − R^{2+} and Al^{IV} − Fe/(Fe + Mg) diagrams are from [30] and [52], respectively.

The tetrahedral and octahedral Al data of the chlorites in the sample of early Ordovician (Tremadocian) parts and of the chlorites from Precambrian, early–middle, and late Ordovician units assembled in two different areas in the Al^{VI} + 2Ti vs. Al^{IV} diagram (Figure 11a,b). Neoformed chlorites are distributed towards the left corner of the Al^{VI} + 2Ti vs. Al^{IV} diagram (Figure 11a), indicating an increase in the dioctahedral substitution (AM, Al^{3+} for Mg^{2+}). Tschermak substitution (TM), e.g., Al^{IV} for Si and Al^{VI} for Mg, indicates higher octahedral substitution. The octhedral-element distribution of chlorites in the Al+□-Mg–Fe diagram refers to completely trioctahedral (Type I) chlorites (Figure 11c,d). Chlorites within the phyllosilicate stacks have slightly greater Fe related to originating from detrital biotites. The chlorites of early Ordovician (Tremadocian) parts are associated with metapelitic rocks, whereas chlorites of the other units are accompanied by both felsic and metapelitic rocks.

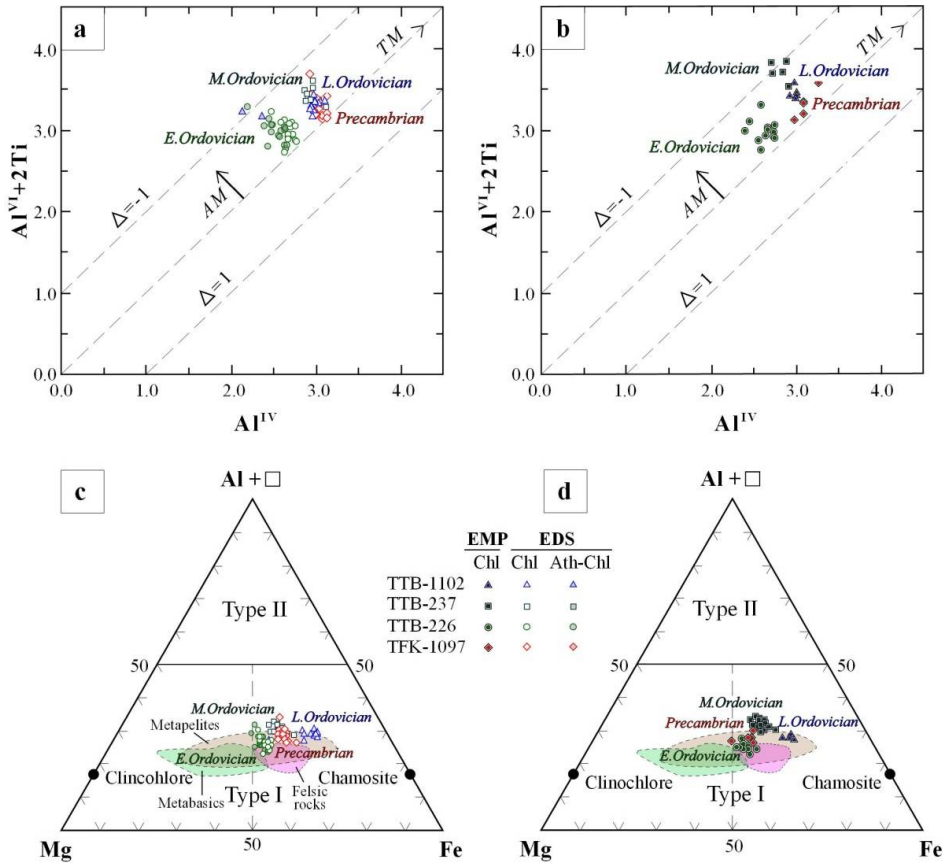

Figure 11. Distribution of chlorite compositions on classification diagrams. (**a**,**b**) Al^{VI} + Ti vs. Al^{IV} [57]; (**c**,**d**) octahedral Al + □–Mg–Fe [58]. (**a**,**c**) and (**b**,**d**) represent the analytical results by EDS and EMP, respectively. Δ = Al^{IV} − Al^{VI} + 2Ti, □ = Octahedral vacancy, Type I = $X_{Mg} + X_{Fe} \geq X_{Al} + X_{□}$, Type II = $X_{Mg} + X_{Fe} < X_{Al} + X_{□}$. The TM and AM arrows point towards increasing Tschermak and dioctahedral substitutions, respectively.

The chlorite thermometry method of [30] was used for temperature estimation (Table 3). Temperature values from chlorite compositions were also obtained from the temperature contours in Si–R^{2+} [31] and Al^{IV}–Fe/(Fe + Mg) diagrams [19] (Figure 10a,b). The temperature estimations of chlorites from these diagrams show a wide range of temperatures from ~150 °C to ≥350 °C (Figure 10a–c). The average temperature data of detrital (CMS) and neoformed chlorites were calculated as 241 °C to ≥350 °C and 201 °C to 268 °C, respectively (Table 3, Figure 12). The temperature conditions of detrital chlorites display differences for individual samples, i.e., detrital chlorites in the samples from the lower parts reveal higher temperature conditions than those of the upper parts. Similarly, the temperature condition

of the neoformed chlorite in the epimetamorphic slate was higher than the low-grade anchimetamorphic slate sample (Figure 12).

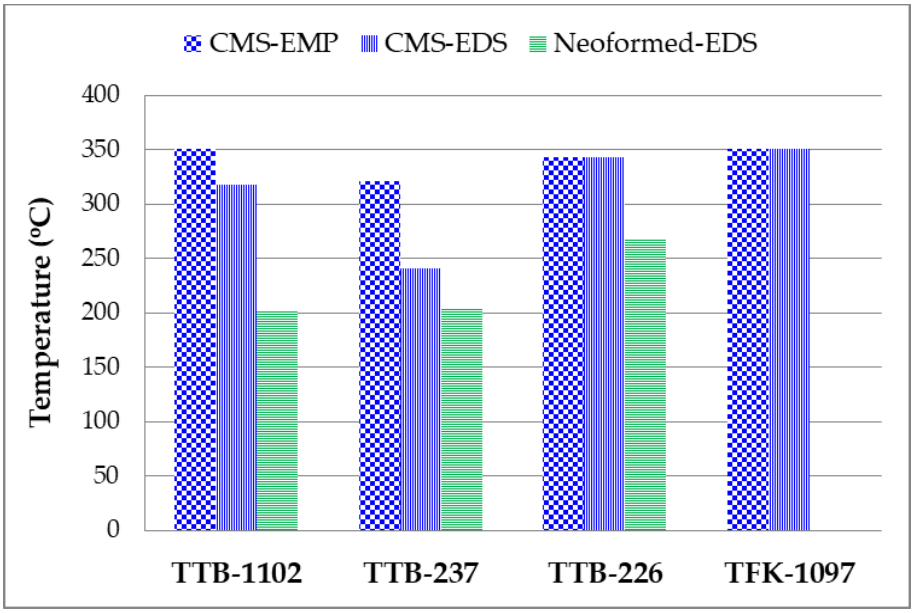

Figure 12. Average temperature distributions of detrital (chlorite–mica stacks-CMS) and neoformed chlorites obtained from EMP and EDS data based on the thermometry method of [28]. Metamorphic grade and stratigraphic depth increase toward the right from low-grade anchizone/late Ordovician (TTB-1102) to epizone/Precambrian (TFK-1097).

The compositional variations of white mica and illite are shown in Table 4, Figure 13. Mineral chemistry studies performed with SEM-BSE images revealed the presence of NaK mica and paragonites, which could not be detected by XRD, in two samples. K-white micas often plot in the compositional space between ideal muscovite and phengite, whereas neoformed illite minerals are projected in the phengitic to celadonitic compositional space in the M^{+}-4Si-R^{2+} diagram (Figure 13a,b). In the Fe + Mg-Al^{IV}–Al^{VI} mica diagram (Figure 13c,d), detrital white micas have muscovitic compositions, but neoformed illite compositions shift to the Fe + Mg corner towards phengite and ferrimuscovite compositions. Tetrahedral Si and total interlayer cation occupancy of detrital K-white micas, NaK micas, and neoformed illites are clearly distinguished in the Si−(Na + K) diagram (Figure 13e,f).

Illites have relatively higher Si-, Fe-, and Mg- and lower K-content than K-white micas. The distributions of octahedral Fe, Mg, and interlayer Na content in neoformed illites with respect to white micas in the Precambrian unit are remarkably different from other units. Contrary to detrital white micas, neoformed illites in the Precambrian unit have lower Fe- and Mg- content but higher interlayer Na-content. NaK micas are distinguished by lower Si-, Fe-, Mg- and higher Al- content than muscovite and illite, in addition to higher interlayer Na content (Figure 13a–f).

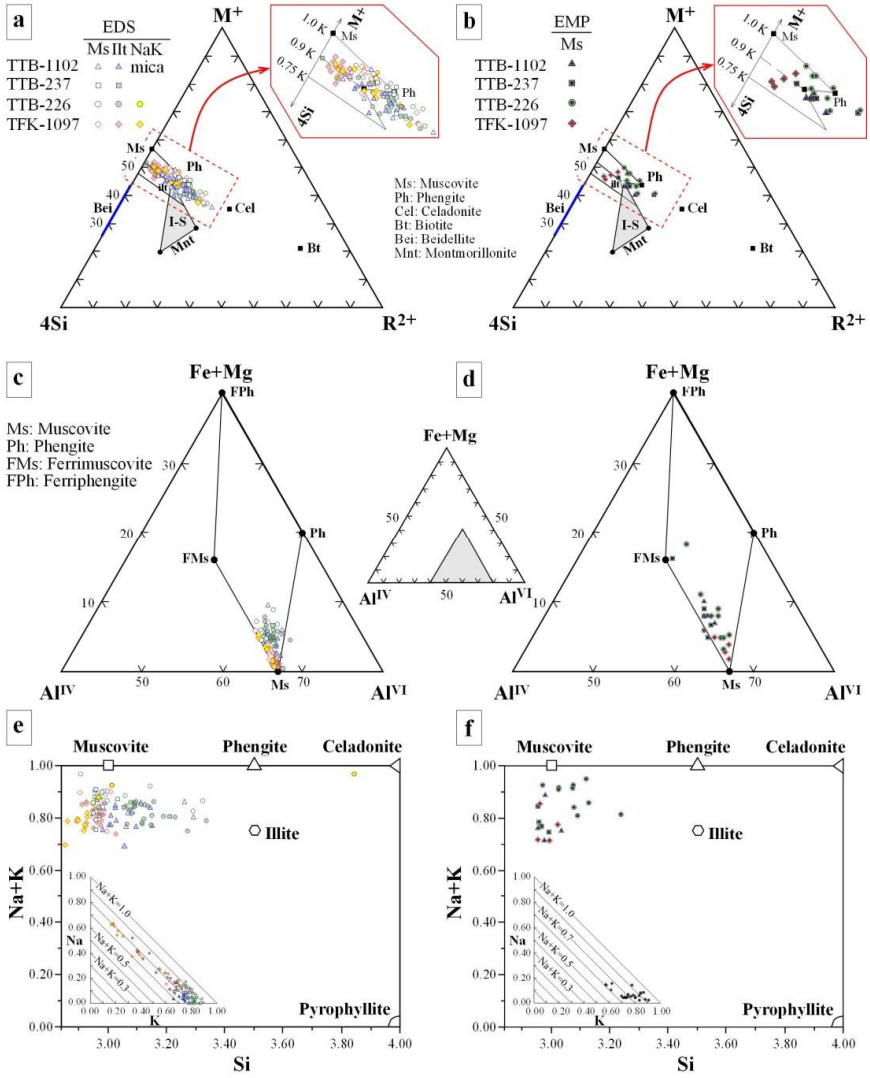

Figure 13. The compositional distributions of illites/micas. (**a**,**b**) M^+–4Si–R^{2+} triangular diagram [59], (**c**,**d**) Fe + Mg–Al^{IV}-Al^{VI} [60], (**e**,**f**) Na + K vs. Si diagram.

5. Discussion

5.1. Chlorite Chemistry

Chlorite composition can be sensitive to the diagenetic/metamorphic grade. The tetrahedral Al (Al^{IV}) and octahedral R^{2+} (Mg and Fe^{2+}) contents of chlorite increase with increasing grade [13–20]. Thus, different chemical compositions for detrital (metamorphic) and authigenic (diagenetic) chlorites have been reported in many studies (e.g., [17,21–24].

Chlorites in studied samples exhibit different compositions for the samples which have different metamorphic grades. Tetrahedral Al and octahedral Fe + Mg increase, whereas octahedral Al decreases together with the increasing grade of metamorphism. Chlorites metasiltstone and slate samples from Precambrian–Early Ordovician (Tremadocian) parts have ripidolite, whereas metasandstone and slate samples from the early–middle Ordovician–Silurian have brunsvigite compositions. It has been noticed that the chlorites in Tremadocian (early Ordovician) metaclastics have different compositions with respect to the others. It was evaluated that this difference is related not only to the metamorphic grade but also to different detrital origins. The chemistry data of chlorites indicating a different source for early Ordovician (see Figure 11b) also support this opinion.

Neoformed chlorites have higher Si-but lower Al^{IV}- and Fe-contents than those detrital (CMS) chlorites. The greater Fe content of chlorites in CMS seems to be related to originating

from biotites. During the alteration of biotites to chlorite, the released excess Fe ions [61–63] could be precipitated as iron oxides and/or sulfur (i.e., hematite, pyrite).

Chlorite geothermometry data for detrital and neoformed origin (Figure 12) are well-matched with KI data (Figure 14), as well as with the textural (slaty cleavage) and other mineralogical (phyllosilicate mineral associations, polytype) maturation data. The different temperature data for detrital (higher temperature) and neoformed (lower temperature) chlorites indicate that the detrital chlorites preserve their metamorphic nature even in anchizonal conditions.

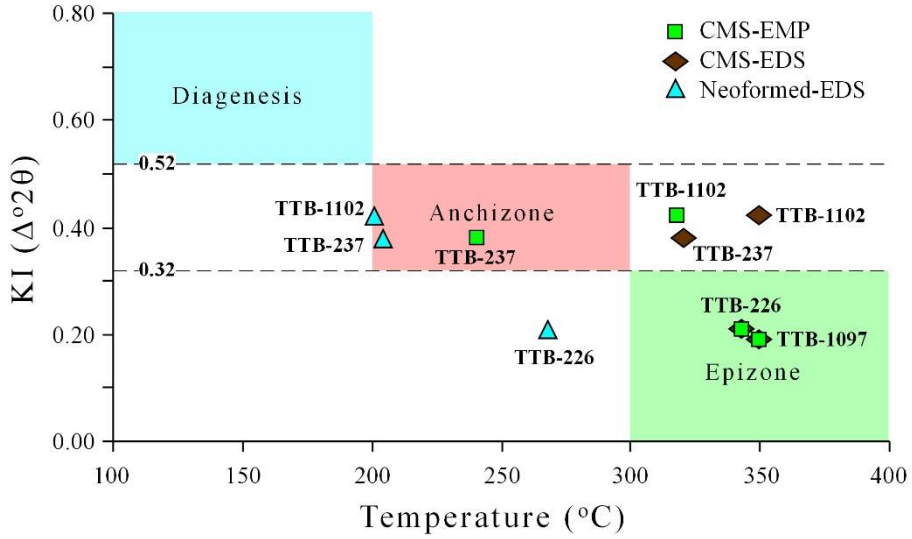

Figure 14. Chlorite thermometry data versus illite Kübler index data of the samples. The Diagenesis–Anchizone–Epizone regions are drawn based on assumed temperature limits for low and upper limits of anchizone [2,7–9].

5.2. Illite/White Mica Chemistry

Illite/mica compositions display the ranges among muscovite–phengite–celadonite. Illites with neoformation origins represent phengitic, whereas micas have commonly muscovitic and partly paragonitic and celadonitic compositions. Tetrahedral Al and interlayer K + Na contents of illite/micas increase together with the increasing grade of diagenesis-metamorphism and change the compositions from illite and phengite to ideal muscovite. Increasing the interlayer K^+ content and layer charge (especially tetrahedral charge) during the transformation from illite to muscovite, together with the increasing diagenesis/metamorphism, are known in the literature [11,25].

In compensation for tetrahedral-charge change, octahedral-charge increases because of the Fe^{2+} and Mg substitutions for Al^{VI}. An increase in Fe^{2+} and Mg (or phengitic) content is mainly related to temperature-related diagenetic-metamorphic grade [10–12,64] but may also be associated with changes in the composition of diagenetic/metamorphic solutions [15,60]. The higher Fe and Mg contents of neoformed illite should be related to Mg- and Fe-rich diagenetic solutions, derived from the conversion of biotite to chlorite and then C-V, as stated for the Fe-rich (chamositic) chlorites.

NaK mica and paragonite-bearing samples in the Precambrian and Lower Ordovician units are restricted to high anchizonal–epizonal grades. Their occurrences are characteristic for the extensional basins [46,65], where the temperature is dominant, which are observed as replacement type developments within the detrital CMS [25]. Na,K-mica were developed within the CMS, amongst the {001} layers of muscovite (see Figure 4e,f). This occurrence may be related to the replacement of muscovite with Na-rich solutions. Retrograde or second metamorphic recrystallization occurrences of paragonite and/or mixed Na,K-mica were documented in the early Paleozoic sedimentary unit [25,66,67].

6. Conclusions

The Precambrian–Early Paleozoic metaclastic rocks of the Eastern Tauride Belt were metamorphosed under low temperature (low anchizone to epizone) conditions. In addition to textural and mineralogical changes, the mineral chemistry of phyllosilicates also affected the metamorphism. Under low-temperature metamorphic conditions, detrital biotite–muscovite stacks altered to CMS, in which the chlorites were derived from biotites, and therefore their composition is rich in Fe (chamosite). In addition to the transformation of clastic phyllosilicates, phyllosilicate neoformation processes have also taken place. The neoformed illites and chlorites were formed in the matrix, whereas replacement type NaK mica and paragonite minerals are also developed within the {001} planes of muscovites in CMS. Neoformed chlorites have higher Si but lower Al^{IV} and Fe contents than detrital (CMS) chlorites. The chlorite geothermometry data indicate that the calculated temperature values are compatible with the metamorphic grades. The increasing degree of metamorphism was reflected in the chlorite geothermometer, in other words, in the chlorite chemistry. In terms of the effect of metamorphism grade on the illite/mica composition, tetrahedral Al and interlayer K + Na contents of illite/micas increase together with the increasing grade of diagenesis-metamorphism and change the compositions from illite and phengite to ideal muscovite. The variations of phyllosilicate mineral chemistry data in accordance with the textural and mineralogical data indicate that the mineral chemistry data of phyllosilicate can be used as a useful tool for low-temperature metamorphic petrology.

Author Contributions: Investigation, Ö.B., H.Y.; formal analysis, Ö.B.; writing—original draft preparation, Ö.B.; resources, Ö.B., H.Y. All authors have read and agreed to the published version of the manuscript.

Funding: This research was funded by the Research Fund of Cumhuriyet University, part of Project Number M-469.

Acknowledgments: The authors also acknowledge the contributions of Paul Schroeder, Doug Crowe, Chris Fleischer, and John P. Schields from the University of Georgia (Athens, Georgia, USA) in terms of the electron microscope and electron microprobe analyses. The authors are also grateful to the editorial office and two anonymous referees for their constructive comments leading to important improvements in the manuscript.

Conflicts of Interest: The authors declare no conflict of interest.

References

1. Robinson, D. Transition from diagenesis to metamorphism in extensional and collision settings. *Geology* **1987**, *15*, 866–869. [CrossRef]
2. Merriman, R.J.; Frey, M. Patterns of very low grade metamorphism in metapelitic rocks. In *Low-Grade Metamorphism*; Frey, M., Robinson, D., Eds.; Blackwell Science: Oxford, UK, 1999; pp. 61–107.
3. Voll, G. New work on petrofabrics. *Liverp. Manch. Geol. J.* **1960**, *2*, 503–567. [CrossRef]
4. Craig, J.; Fitches, W.R.; Maltman, A.J. Chlorite-mica stacks in low-strain rocks from Central Wales. *Geol. Mag.* **1982**, *119*, 243–256. [CrossRef]
5. Giorgetti, G.; Memmi, F.; Nieto, F. Microstructures of intergrown phyllosilicate grains from Verrucano metasediments (northern Apennines, Italy). *Contrib. Mineral. Petrol.* **1997**, *128*, 127–138. [CrossRef]
6. Kisch, H.J. Mineralogy and petrology of burial diagenesis (burial metamorphism) and incipient metamorphism in clastic rocks. In *Diagenesis in Sediments and Sedimentary Rocks*; Larsen, G., Chilingar, G.V., Eds.; Elsevier: Amsterdam, The Netherlands, 1983; Volume 2, pp. 289–493; 513–541.
7. Frey, M. Very low-grade metamorphism of clastic sedimentary rocks. In *Low Temperature Metamorphism*; Frey, M., Ed.; Blackie & Son: Glasgow, UK, 1987; pp. 9–58.
8. Merriman, R.J.; Peacor, D.R. Very low-grade metapelites: Mineralogy, microfabrics and measuring reaction progress. In *Low-Grade Metamorphism*; Frey, M., Robinson, D., Eds.; Blackwell Science: Oxford, UK, 1999; pp. 10–60.
9. Ferreiro-Mählmann, R.; Bozkaya, Ö.; Potel, S.; Le Bayon, R.; Nieto, F. The pioneer work of Bernard Kübler and Martin Frey in very low-grade metamorphic terranes: Paleo-geothermal potential of variation in Kübler-Index/organic matter reflectance correlations. A review. *Swiss J. Geosci.* **2012**, *105*, 121–152. [CrossRef]
10. Ireland, B.J.; Curtis, C.D.; Whiteman, J.A. Compositional variation within some glauconites and illites and implications for their stability and origins. *Sedimentology* **1983**, *30*, 769–786. [CrossRef]

11. Hunziker, J.C.; Frey, M.; Clauer, N.; Dallmeyer, R.D.; Fredrichsen, H.; Flehmig, W.; Hochstrasser, K.; Roggviler, P.; Schwander, H. The evolution of illite to muscovite: Mineralogical and isotopic data from the Glarus Alps. Switzerland. *Contrib. Mineral. Petrol.* **1986**, *92*, 157–180. [CrossRef]
12. Brill, B.A. Illite crystallinity, b0 and Si content of K-white mica as indicators of metamorphic conditions in low-grade metamorphic rocks at Cobar, New South Wales. *Aust. J. Earth Sci.* **1988**, *35*, 295–302. [CrossRef]
13. Weaver, C.E. *Shale Slate Metamorphism in Southern Appalachians*; Elsevier: Amsterdam, The Netherlands, 1984.
14. Cathelineau, M.; Nieva, D.A. Chlorite solid solution geothermometer, the Los Azufres geothermal system (Mexico). *Contrib. Mineral. Petrol.* **1985**, *91*, 235–244. [CrossRef]
15. Cathelineau, M. Cation site occupancy in chlorites and illites as a function of temperature. *Clay Miner.* **1988**, *23*, 471–485. [CrossRef]
16. Velde, B.; Medhioub, M. Approach to chemical equilibrium in diagenetic chlorites. *Contrib. Mineral. Petrol.* **1988**, *98*, 122–127. [CrossRef]
17. Hillier, S.; Velde, B. Octahedral occupancy and the chemical composition of diagenetic (low temperature) chlorites. *Clay Miner.* **1991**, *26*, 149–168. [CrossRef]
18. Jahren, J.S.; Aagard, P. Diagenetic illite-chlorite assemblages in arenites. I. Chemical evolution. *Clays Clay Miner.* **1992**, *40*, 540–546. [CrossRef]
19. Xie, X.G.; Byerly, G.R.; Ferrell, R.E. IIb trioctahedral chlorite from the Barberton greenstone belt: Crystal structure and rock composition constraints with implications to geothermometry. *Contrib. Mineral. Petrol.* **1997**, *126*, 275–291. [CrossRef]
20. Potel, S.; Ferreiro-Mählmann, R.; Stern, W.B.; Mullis, J.; Frey, M. Very low-grade metamorphic evolution of pelitic rocks under high-pressure/low-temperature condition, NW New Caledonia (SW Pacific). *J. Petrol.* **2006**, *47*, 991–1015. [CrossRef]
21. Hillier, S.; Velde, B. Chlorite interstratified with a 7 Å mineral: An example from offshore Norway and possible implications for the interpretation of the composition of diagenetic chlorites. *Clay Miner.* **1992**, *27*, 475–486. [CrossRef]
22. Hillier, S. Origin, diagenesis, and mineralogy of chlorite minerals in Devonian lacustrine mudrocks, Orcadian Basin, Scotland. *Clays Clay Miner.* **1993**, *41*, 240–259. [CrossRef]
23. Jiang, W.T.; Peacor, D.R. Formation of corrensite, chlorite and chlorite-mica stacks by replacement of detrital biotite in low-grade pelitic rocks. *J. Metamorph. Geol.* **1994**, *12*, 867–884. [CrossRef]
24. Bartier, D.; Buatier, M.; Lopez, M.; Potdevin, J.L.; Chamley, H.; Arostegui, J. Lithological control on the occurrence of chlorite in the diagenetic Wealden complex of the Bilbao anticlinorium (Basco-Cantabrian Basin, Northern Spain). *Clay Miner.* **1998**, *33*, 317–332. [CrossRef]
25. Bozkaya, Ö.; Yalçın, H.; Schroeder, P.A. Two-step mode of clay formation in the extensional basins: Cambrian–Ordovician clastic rocks of the Antalya unit, SW Turkey. *Clay Miner.* **2017**, *52*, 365–389. [CrossRef]
26. Inoue, A.; Meunier, A.; Patrier-Mas, P.; Rigault, C.; Beaufort, D.; Vieillard, P. Application of chemical geothermometry to low-temperature trioctahedral chlorites. *Clays Clay Miner.* **2009**, *57*, 371–382. [CrossRef]
27. Inoue, A.; Inoué, S.; Utada, M. Application of chlorite thermometry to estimation of formation temperature and redox conditions. *Clay Miner.* **2018**, *53*, 143–158. [CrossRef]
28. Bourdelle, F.; Parra, T.; Chopin, C.; Beyssac, O. A new chlorite geothermometer for diagenetic to low-grade metamorphic conditions. *Contrib. Mineral. Petrol.* **2013**, *165*, 723–735. [CrossRef]
29. Lanari, P.; Wagner, T.; Vidal, O. A thermodynamic model for di-trioctahedral chlorite from experimental and natural data in the system MgO-FeO-Al_2O_3- SiO_2-H_2O: Applications to P-T sections and geothermometry. *Contrib. Mineral. Petrol.* **2014**, *167*, 968. [CrossRef]
30. Bourdelle, F. Low-temperature chlorite geothermometry and related recent analytical advances: A review. *Minerals* **2021**, *11*, 130. [CrossRef]
31. Bourdelle, F.; Cathelineau, M. Low-temperature chlorite geothermometry: A graphical representation based on a T-R^{2+}-Si diagram. *Eur. J. Mineral.* **2015**, *27*, 617–626. [CrossRef]
32. Göncüoglu, M.C.; Dirik, K.; Kozlu, H. General characteristics of pre-Alpine and Alpine Terranes in Turkey: Explanatory notes to the terrane map of Turkey. Annales Geologique de Pays Hellenique. *Geol. Soc. Greece* **1997**, *37*, 515–536.
33. Şengör, A.M.C.; Yılmaz, Y. Tethyan evolution of Turkey: A plate tectonic approach. *Tectonophysics* **1981**, *75*, 181–241. [CrossRef]
34. Özgül, N. Some geological aspects of the Taurus orogenic belt (Turkey). *Bull. Geol. Soc. Turk.* **1976**, *19*, 65–78. (In Turkish with English Abstract)
35. Özgül, N.; Metin, S.; Dean, W.T. Lower Paleozoic stratigraphy and faunas of the Eastern Taurus mountains in the Tufanbeyli region, southern Turkey. *Bull. Miner. Res. Explor.* **1973**, *79*, 9–20.
36. Bozkaya, Ö.; Yalçın, H.; Göncüoglu, M.C. Mineralogic and organic responses to the stratigraphic irregularities: An example from the lower Paleozoic very low-grade metamorphic units of the eastern Taurus Autochthon, Turkey. *Schweiz. Mineral. Petrogr. Mitt.* **2002**, *82*, 355–373.
37. Göncüoğlu, M.C.; Göncüoğlu, Y.; Kozur, H.W.; Kozlu, H. Paleozoic stratigraphy of the Geyik Dağı unit in the eastern Taurides (Turkey): New age data and implications for Gondwanan evolution. *Geol. Carpath.* **2004**, *55*, 433–447.
38. Metin, S.; Ayhan, A.; Papak, I. Geology of the western part of the eastern Taurus (SSE Turkey). *Bull. Miner. Res. Explor.* **1987**, *107*, 1–12. (In Turkish)

39. Erkan, E.; Özer, S.; Sümengen, M.; Terlemez, I. *Basic Geology of the Area Between Sarız-Şarkısla-Gemerek-Tomarza*; M.T.A. Report No. 6546; Institute of Mineral Research and Exploration: Ankara, Turkey, 1978. (In Turkish)
40. Demirtaşlı, E.; Metin, S.; Ayhan, A. Stratigraphy of the eastern Taurus Autochthon. In Proceedings of the International Symposium on the Geology of the Taurus Belt, Ankara, Turkey, 26–29 September 1983; pp. 7–16.
41. Kozlu, H.; Göncüoglu, M.C. Stratigraphy of the Infracambrian rock-units in the Eastern Taurides and their correlation with similar units in southern Turkey. In *Lower Palaeozoic Evolution in Northwest Gondwana*; Göncüoğlu, M.C., Derman, A.S., Eds.; Turkish Association Petroleum Geologists Special Publication: Ankara, Turkey, 1997; Volume 3, pp. 50–61.
42. Monod, O.; Kozlu, H.; Ghienne, J.-F.; Dean, W.T.; Günay, Y.; Le Hérissé, A.; Paris, F.; Robardet, M. Late Ordovician glaciation in southern Turkey. *Terra Nova* **2003**, *15*, 249–257. [CrossRef]
43. Armstrong, J.T. Quantitative analysis of silicate and oxide materials: Comparison of Monte Carlo, ZAF, and phi-rho-z procedures. In *Microbeam Analysis*; Newbury, D.E., Ed.; San Francisco Press: San Francisco, CA, USA, 1988; pp. 239–246.
44. Armstrong, J.T. CITZAF: A package of correction programs for the quantitative electron microbeam X-ray analysis of thick polished materials, thin films, and particles. *Microbeam Anal.* **1995**, *4*, 177–200.
45. Kisch, H.J. Development of slaty cleavage and degree of very-low-grade metamorphism: A review. *J. Metamorph. Geol.* **1991**, *9*, 735–750. [CrossRef]
46. Merriman, R.J. Clay minerals and sedimentary basin history. *Eur. J. Mineral.* **2005**, *17*, 7–20. [CrossRef]
47. Bozkaya, Ö.; Gürsu, S.; Göncüoglu, M.C. Textural and mineralogical evidence for a Cadomian tectonothermal event in the eastern Mediterranean (Sandıklı-Afyon area, western Taurides, Turkey). *Gondwana Res.* **2006**, *10*, 301–315. [CrossRef]
48. Kübler, B. Evaluation quantitative du métamorphisme par la cristallinité de l'illite. *Bull. Centre Rech. Pau-SNPA* **1968**, *2*, 385–397.
49. Sassi, F.P.; Scolari, A. The b_0 value of the potassic white micas as a barometric indicator in low-grade metamorphism of pelitic schists. *Contrib. Mineral. Petrol.* **1974**, *45*, 143–152. [CrossRef]
50. Guidotti, C.V.; Sassi, F.P. Classification and correlation of metamorphic facies series by means of muscovite b0 data from low-grade metapelites. *Neues Jahrb. Mineralogie. Abh.* **1986**, *153*, 363–380.
51. Weaver, C.E.; Pollard, L.D. The chemistry of clay minerals. In *Developments in Sedimentology*, 15th ed.; Elsevier: Amsterdam, The Netherlands, 1973; p. 272.
52. Bailey, S.W. Summary of recommendations of AIPEA nomenclature committee on clay minerals. *Am. Mineral.* **1980**, *65*, 1–7. [CrossRef]
53. Wiewióra, A.; Weiss, Z. Crystallochemical classifications of phyllosilicates based on the unified system of projection of chemical composition: II. The chlorite group. *Clay Miner.* **1990**, *25*, 83–92. [CrossRef]
54. Hayes, J.B. Polytypism of chlorite in sedimentary rocks. *Clays Clay Miner.* **1970**, *18*, 285–306. [CrossRef]
55. Foster, M.D. Interpretation of the composition and a classification of the chlorites. *US Geol. Surv. Prof. Pap.* **1962**, *414*, 1–33.
56. Curtis, C.D.; Hughes, C.R.; Whiteman, J.A.; Whittle, C.K. Compositional variations within some sedimentary chlorites and some comments on their origin. *Mineral. Mag.* **1985**, *49*, 375–386. [CrossRef]
57. Zane, A.; Weiss, Z. A procedure for classification of rock-forming chlorites based on microprobe data. *Rend. Fis. Acc. Lincei.* **1998**, *9*, 51–56. [CrossRef]
58. Zane, A.; Sassi, R.; Guidotti, C.V. New data on metamorphic chlorite as a petrogenetic indicator mineral, with special regard to greenschist facies rocks. *Canad. Mineral.* **1998**, *36*, 713–726.
59. Meunier, A.; Velde, B. *Illite. Origins, Evolution and Metamorphism*; Springer: Berlin, Germany, 2004; p. 286.
60. Guidotti, C.V. Micas in metapelitic rocks. In *Micas. Reviews in Mineralogy 13*; Bailey, S.W., Ed.; Mineralogical Society of America: Washington, DC, USA, 1984; pp. 357–467.
61. Parry, W.T.; Downey, L.M. Geochemistry of hydrothermal chlorite replacing igneous biotite. *Clays Clay Miner.* **1982**, *30*, 81–90. [CrossRef]
62. Veblen, D.R.; Ferry, J.M. A TEM study of the biotite-chlorite reaction and comparison with petrologic observations. *Am. Mineral.* **1983**, *68*, 1160–1168.
63. Eggleton, R.A.; Banfield, J.F. The alteration of granitic biotite to chlorite. *Am. Mineral.* **1985**, *70*, 902–910.
64. Robinson, D.; Nicholls, R.A.; Thomas, L.J. Clay mineral evidence for low-grade Caledonian and Variscan metamorphism in south-western Dyfed, South Wales. *Mineral. Mag.* **1980**, *43*, 857–863. [CrossRef]
65. Merriman, R.J. Clay mineral assemblages in British Lower Paleozoic mudrocks. *Clay Miner.* **2006**, *41*, 473–512. [CrossRef]
66. Árkai, P. Very low- and low-grade Alpine regional metamorphism of the Paleozoic and Mesozoic formations of the Bükkium, NE-Hungary. *Acta Geol. Hung.* **1983**, *26*, 83–101.
67. Árkai, P.; Abad, I.; Nieto, F.; Németh, T.; Horváth, P.; Kis, V.K.; Judik, K.; Jiménez-Millán, J. Retrograde alterations of phyllosilicates in low-grade metapelite: A case study from the Szendrő Paleozoic, NE-Hungary. *Swiss J. Geosci.* **2012**, *105*, 263–282. [CrossRef]